Journal of Materials Chemistry A

Accepted Manuscript

ROYAL SOCIETY OF CHEMISTRY

www.rsc.org/materialsA

Journal Name

ARTICLE

Stalagmite-like Self-cleaning Surfaces Prepared by Silanization of Plasma-assisted Metal-oxide Nanostructures

Received 00th January 20xx,
Accepted 00th January 20xx

DOI: 10.1039/x0xx00000x

www.rsc.org/

Ching-Yu Yang, [a] Shang-I Chuang, [a] Yu-Hsiang Lo, [a] Hsin-Ming Cheng,[b*] Jenq-Gong Duh [a] and Po-Yu Chen [a*]

Effective self-cleaning coatings with liquid repellency are crucial for eliminating surface contamination and reducing drag force, which enables wide industrial applications. However, most coatings are fabricated through complicated and expensive processes that limit mass production capability. To overcome this limitation, we designed a simple methodology based on the atmospheric-pressure-plasma-assisted fabrication. The hierarchically-structured, stalagmite-like tungsten oxide (WO_{3-x}) coatings were synthesized within a few seconds. After silanization, the coatings not only obtained the cost-effective superhydrophobic surfaces achieving high static contact angle toward water (160 ° ± 2 °, surface tension γ = 72.8 dyn/cm), but showed oleophobicity toward liquids with lower surface tension ranging from 64 to 27.5 dyn/cm. Additionally, the two-tier topography decorated with fluoroalkylsilane traps air cushions within the textures contributing low sliding angle (< 2°) and low contact angle hysteresis toward both water and glycerol. The robust Cassie state can even sustain high impact velocity of a liquid drop exceeding 2 m/s. Moreover, the coatings exhibited superior self-cleaning abilities and performed multi-functionally regarding high transparency, flexibility, mechanical and thermal stability. The growth mechanism of hierarchical WO_{3-x} and dynamic behavior of liquid droplets on the coatings were also investigated in this study. These micro- and nano-structures which were constructed at room-temperature enable the seamless integration on not only the brittle substrates but various flexible substrates, such as plastic films and fibrous papers, without sacrificing performance.

Introduction

Self-cleaning coatings have attracted considerable attention over the last decade as the broadened range of perspective industrial applications they present.[1-6] Since the discovery of the "lotus effect" by Barthlott and Neinhuis,[7] an accelerating number of artificial superhydrophobic surfaces have been developed. [8-13] Common to superhydrophobic surface is that the continuous solid/gas arises from the topography with roughness on the nano- and micrometre scale combined with a low surface energy.[14] This combination accomplishes the anti-adhesive behavior toward water. Apart from superhydrophobicity, oleophobicity is an emerging topic that extends the anti-adhesive properties of the surface toward low-surface tension liquids.[5, 15-20]

Additional applicabilities such as transparency,[4, 18, 20-24] flexibility,[18, 23, 24] and chemical and thermal stability,[4, 22, 25] have been widely investigated for a wide range of practical applications for antireflective coatings, self-cleaning windows, electronic device protection. In addition, some studies have discovered that superhydrophobicity can benefit anti-icing applications as reducing ice adhesion strength or delaying ice nucleation.[26-28] However, the fulfillment of this multifunctional requirement renders the design of self-cleaning surfaces more challenging. Expensive and complex processes as well as high synthesizing temperatures are typically required that have limited the versatile integration and continuous production of self-cleaning coatings. In this study, we developed a novel and facile method that combines an atmospheric pressure plasma (APP) technique with silanization to synthesize stalagmite-like, transparent, and self-cleaning surfaces for the first time. Self-cleaning coatings developed through silanization and plasma-assisted metal oxide nanostructures are quite distinct from the coatings developed by existing plasma polymerization techniques.[24] Plasma polymerization has been reported as a succinct method[24] for fabricating self-cleaning surfaces. Hierarchically-structured rough and hydrophobic polymeric layer could be obtained simultaneously through the polymerization of specific monomers. However, a lengthy coating cycle and unstable wettability are the drawbacks that limit the practical applications.[24, 29] To overcome these problems, we utilized the APP technique for fabricating complex structures within a few seconds, which is considerably shorter than that of conventional techniques such as replication,[30] coating,[31] chemical etching,[32] and lithography.[33] Meanwhile, this technique established a satisfactory template for silanization to effectively entrap air cushions. Thus, the synthesized coatings exhibited

[a] Department of Materials Science and Engineering, National Tsing Hua University, Hsinchu 101, Sec. 2, Kuang-Fu Rd., Hsinchu 30013, Taiwan
[b] Material and Chemical Research Laboratories, Industrial Technology Research Institute, 195, Sec. 4, Chung Hsing Rd., Chutung, Hsinchu 31040, Taiwan
*Corresponding authors: SMCheng@itri.org.tw; poyuchen@mx.nthu.edu.tw
†Electronic Supplementary Information (ESI) available: [details of any supplementary information available should be included here]. See DOI: 10.1039/x0xx00000x

oleophobicity toward ethylene glycol and n-hexadecane and low sliding angle (< 2°) toward water and glycerol. Additionally, we provide a solution herein for developing a new multi-functional self-cleaning surface that is mechanically and thermally stable and transparent. The synthesized coatings demonstrated the ability to withstand environments with high temperature or high humidity. They even maintained the self-cleaning property after sand abrasion tests. The discussion regarding long-term durability for prolonged continuous exposure of silanized surface to water, which has seldom been performed, was also included. Moreover, the entire process is conducted at atmospheric pressure and room temperature, thus has been demonstrated to be substrate-independent on various substrates such as glass, paper, stainless steel and plastic substrates.

Experimental Section

Customized Atmospheric Pressure Plasma System

Plasma jet consists of a center high-voltage electrode made of pure tungsten rod (1 mm in diameter) and an outer stainless steel nozzle which provides grounding. The powered center electrode is connected to a radio frequency power supply (13.6 MHz) associated with an automatic matching unit to insure the maximum power output. The thickness of the gas gap is 1 mm. The plasma jet, which is with the diameter of 2-3 mm and the length of approximately 1 cm, is generated in the nozzle and blown out by the gas flow. The working gas is composed of 0.2 % v/v oxygen in high purity argon for plasma ignition under the power of 50 W. The gas flow rates of argon and oxygen are measured as 15 standard liter per minute (slm) and 40 standard cubic centimeters per minute (sccm), respectively. Argon and oxygen mixed before supplying to the plasma jet are fed by using separate pipes and flow meters to control the optimal flow rate. The distance between the jet and the substrate is controlled at 2 mm.

Coating Procedure

The substrates (1.5×1.5 cm^2) were loaded on the stage in the plasma chamber. A bluish glow discharge appeared from the apex of nozzle when injecting the working gas and applying power. The generated plasma jet scanned through the whole area of substrates under identical scanning rate (0.8 sec/cm^2), and deposited a brownish layer covering on the surface. The treated substrates were put into the glass vessels containing 4 μL of 1H, 1H, 2H, 2H-perfluorodecyltriethoxysilane (FAS-17, $[CF_3(CF_2)_7\text{-}CH_2\text{-}CH_2Si(OCH_3)_3]$) as FAS precursor. The reagent with the highest commercial-available purity was purchased from Sigma-Aldrich® (USA). After FAS modification process at 17-25 ℃ for 1 h, the colourless coating with superior superhydrophobicity and oleophobicity was obtained. Additionally, the adhesion of the self-cleaning coating to the substrates was investigated. The coating was neither damaged by sand abrasion test nor removed by stream of water (Fig. S1). The water feed rate was controlled at 25 ml/min, and the corresponding droplet frequency was about 200 drops/min. The diameter of each water droplet was 3 mm. The impact height was set to be 5 cm which is the distance from the outlet of the water pipe to the surface of substrates. The self-cleaning coating could sustain at least 600 s under water stream. The reproducibility was confirmed by repeating the identical procedure for more than five times on various substrates such as polished silicon, glass slide, stainless steels, PET films, and papers.

Material Characterization

The microstructure and morphology of coatings were characterized by field emission scanning electron microscopy (FE-SEM) (HITACHI SU8010, Japan), transmission electron microscopy (TEM) (JOEL, JEM-2010, Japan) and the topography were observed by atomic force microscopy (AFM) (Bruker BioScope Catalyst, USA). As for the chemical composition analyses of surface coating, X-ray photoelectron spectroscopy (XPS) (PHI 5000 VersaProbe II, USA) using the C 1s peak energy (284.6 eV) as calibrated energy standard and energy-dispersive X-ray spectroscopy (EDX) under TEM were utilized. Optical transmittance spectrum of the glass modified with the self-cleaning coating was measured using a UV–visible-near infrared spectroscopy (UV-Vis-NIR) (HITACHI U-4100, Japan). The amount of FAS decorated upon the hierarchically structured surface was determined by thermogravimetric analysis (TGA) (TA Instruments Discovery TGA, USA).

Contact Angle Measurements

The static contact angle (SCA), roll-off angle and contact angle hysteresis (CAH, i.e. the difference between the advancing angle θ_{adv} and receding angle θ_{rec}) on the as-prepared sample were measured from sessile drops by a contact angle meter equipped with a tilting stage (First Ten Angstrom1000, USA). Deionized water, glycerol (≥ 99 %, Sigma-Aldrich®, USA), ethylene glycol (≥ 99%, J.T.Baker®), and n-Hexadecane (99 %, Alfa Aesar, UK) droplets of 5 μL were deposited manually at room temperature and 50-70 % relative humidity. At least five individual measurements were performed on each modified sample. For the clear observation, the water and n-Hexadecane droplets were stained by Methylene Blue trihydrate (95 %, Acros Organics, USA) and Oil Red O (Acros Organics, USA), respectively.

Dynamic Behaviour Observations of a Water Bouncing Drop

Regarding the characterization of the contact time at the first bounce of water droplets, the top and side views of water drops impact were captured by a high speed camera (Fastec Imaging Co., TS4, USA) separately for the same impact region. Each film was at the frame rate of 5600 frames per second. The radius of the drop was calculated from the average weight of 20 drops measured by precision electronic balance. Water drops of 7.7 μL (the corresponding radius is 1.23 mm) were generated from a fine needle fixed at a height up to 20 cm. The entire experimental set-up was placed in an ambient environment (17-25 ℃ and 50-70% relative humidity). As for the trajectory of a water droplet on the modified U-shaped PET film, the side view of drop rolling was recorded by the high speed camera at the frame rate of 2000 frames per second.

Results and Discussion

Preparation and Characterization of Hierarchically Structured Coatings

Scheme 1a illustrates the working principle and key processes for preparing our self-cleaning coating. The substrates were treated with ethanol and deionized water before the APP process. The cleaned substrates were loaded into a chamber under constant temperature and humidity and were treated with oxygen mixed argon plasma to form a hierarchically rough and porous coating on the substrate surface. The as-synthesized coating at this stage was superhydrophilic (SCA ~ 10°).

Materials with lower solid surface energy tend to have higher SCA according to the Young's equation.[34] Fluorinated materials, fluoroalkylsilane (FAS) for example, are logically chosen for decreasing the surface energy because the trifluoromethyl group ($–CF_3$, 15 dyn/cm) obtains the lowest surface energy[35] compared with other functional groups, such as $–CH_2$ (36 dyn/cm), $–CH_3$ (30 dyn/cm), $–CF_2$ (23 dyn/cm).[36] Therefore, after the vapor deposition of FAS (the chemical structure is illustrated in Scheme 1b), the FAS-modified stalagmite-like protrusions exhibited a high SCA toward water, glycerol and n-Hexadecane. Fig. 1 shows the surface morphologies of the plasma-treated samples with different durations (Fig. 1a to 1d). Within a few seconds, clusters with diameters of 60-200 nm were aggregated from nanoparticles with diameters of 5-10 nm. After silanization, the two-tier structure with FAS decoration exhibited the SCA toward water of 139.1° ± 1.6°, 142.0° ± 1.3°, 157.4° ± 3.2°, and 162.9° ± 2.6° corresponding to plasma treatment durations of 9 s, 13 s, 16 s, and 20 s, respectively (red square in Fig. 1e). In addition, with the increasing deposition duration, the corresponding CAH decreased obviously from approximately 30° to 2° (black triangle in Fig. 1e). Moreover, the corresponding SCA toward n-Hexadecane (red open circle in Fig. 1e) achieved 92.0 ° ± 1.6°, 95.8 ° ± 1.3°, 119.4 ° ± 0.8°, and 130.3 ° ± 0.4°, respectively. These results of the SCA toward liquids showed a strong relationship with the root mean square roughness (R_q) as shown in Fig. S2. The value of R_q increased as the APP treatment time increased. Meanwhile, the standard deviation of R_q was progressively increased because the hierarchically structured stalagmite-like protrusions became more prominent as the treatment time increased.

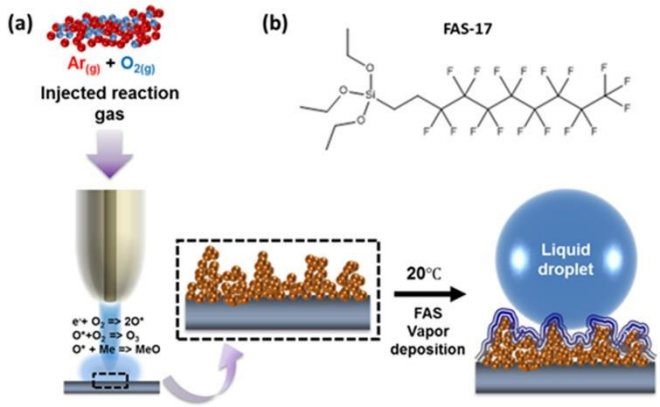

Scheme 1. (a) Illustrations showing the design and development of the transparent self-cleaning surfaces by the combination of APP technique and chemisorption of FAS. (b) The chemical structure of fluoroalkylsilane which is decorated on the hierarchically structured coating.

According to these observations, two-tier topography has a major role in obtaining satisfactory anti-wettability. The micro- and nano-scale structures not only result in the Cassie state, entrapping the air cushions between the asperities but withstand a higher Laplace pressure (i.e., the critical pressure difference at the liquid-gas interface) to avoid the Cassie-to-Wenzel transition.[37] Without surface texture, the SCA toward water and n-Hexadecane on a flat FAS-modified surface were only 130° ± 1.2° and 10° ± 0.8°, respectively. When the deposition duration was longer than 20 s, the SCA toward n-Hexadecane became saturated. Therefore, 20 s was selected as the optimal time in the following tests. The substrate surface was covered with uniform, stalagmite-like hierarchical structures at the micro- and nano-scales after 20 s of deposition (Fig. 1f). The corresponding SCA, CAH, and sliding angle toward various liquids were also measured (Table S1). As shown in the resutls, both water and glycerol exhibited high SCA and low CAH, and sliding angles of less than 2°. The excessive liquid-repellency toward glycerol is demonstrated in the supplemental Video S1. The SCA of ethylene glycol was 150° whereas the corresponding sliding angle is up to40° because of the large contacting solid-liquid area. n-Hexadecane with a surface tension of 27.5 dyn/cm remained attached to the surface even after the substrates were turned upside-down. Accordingly, we concluded that the synthesized self-cleaning surface provided a robust Cassie state for the water and glycerol while induceing a Wenzel state, which led to stronger adhesion when the liquid surface tension was less than 43 dyn/cm.

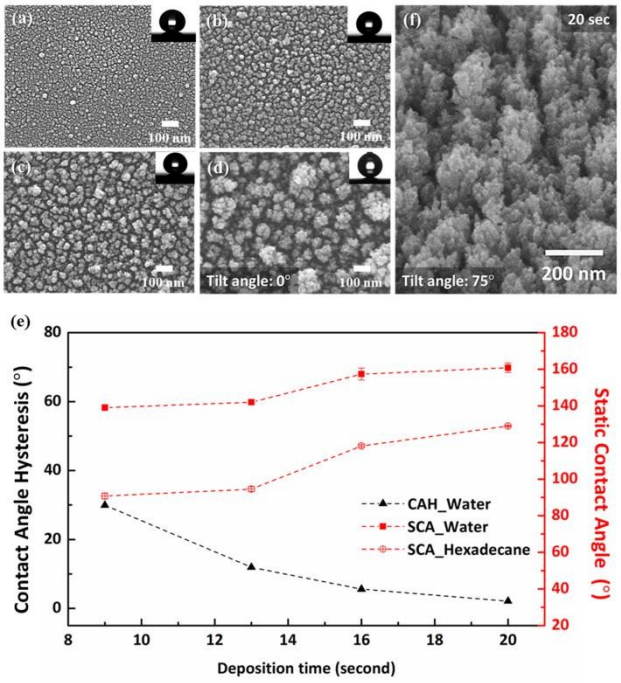

Fig. 1 Top-view SEM images of morphologies and the corresponding SCA toward water (inset) for the samples fabricated by various plasma treatment durations for (a) 9 s, (b) 13 s, (c) 16 s, (d) 20 s. (e) The SCA toward water and n-Hexadecane and contact angle hysteresis (CAH) toward water vary with the deposition time under the APP apparatus. (f) Cross-sectional SEM image of samples treated for 20 s at 75° tilting angle.

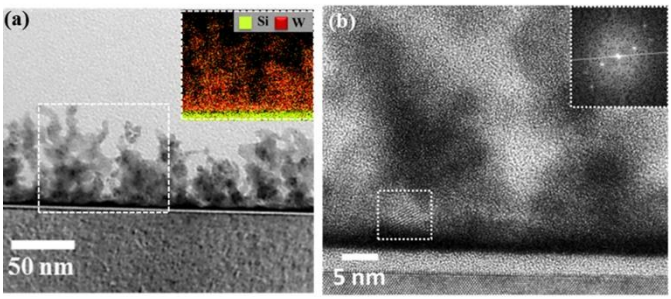

Fig. 2 (a) Cross-sectional TEM images of as-synthesized coating. The major content of deposited coating is tungsten confirmed by EDX (inset). (b) HR-TEM image of as-synthesized coating. Only some of the nanoparticles possessed crystallinity (inset).

To observe the structure of the as-synthesized self-cleaning surface, we first demonstrated this concept by using a silicon substrate with a thin layer of native silicon oxide (SiO_2, 4 nm $\pm$ 1 nm). The as-synthesized coating was characterized by TEM equipped with EDX. The thickness of the as-synthesized porous structure was 58.3 nm $\pm$ 4.2 nm, and the major signal under EDX corresponded to tungsten (Fig. 2a). Because of the high deposition rate and room temperature process in the APP system, most of the deposited nanoparticles showed an amorphous phase and only few nanoparticles exhibited weak crystallinity (Fig. 2b).

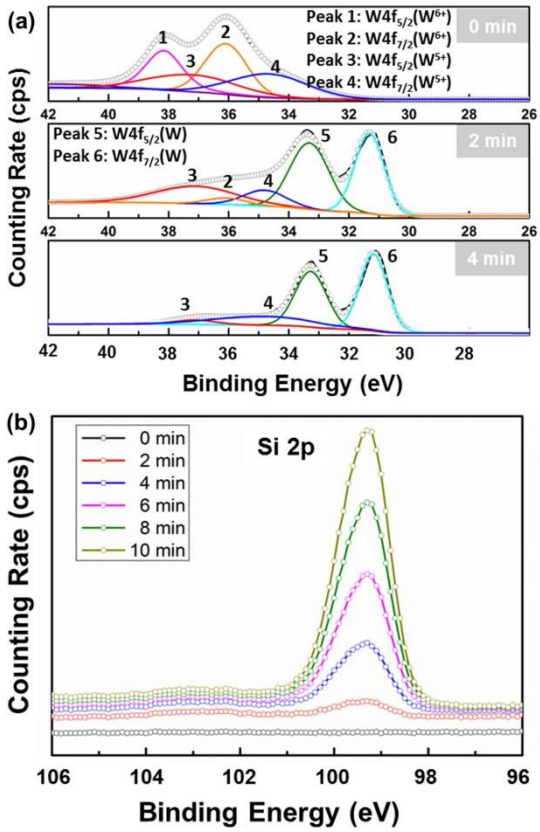

Fig. 3 XPS spectra of (a) W 4f and (b) Si 2p under different sputtering durations by Ar^+ ion. The signal of $W4f_{5/2}$ (33.3 eV) and $W4f_{7/2}$ (31.2 eV) contributed by tungsten increased obviously after sputtering for 4 min. Meanwhile, the signal of Si 2p from Si (99.4 eV) increased gradually. The analyses indicated that the porous WO_{3-x} coatings were removed after sputtering for 4 min and the Si substrate was revealed.

In the past decade, a few studies[38-40] have investigated a series of nanomaterials with well-tailored chemical compositions and nano-architectures directly grown on substrate surface by atmospheric microplasma-assisted nanofabrication. In 2006, Yoshiki et al. first used a tungsten wire as a source for depositing tungsten oxide nanoparticles.[40] The results revealed that the oxidation state of tungsten oxide nanoparticles varied with the oxygen flow rate. To intuitively determine the composition of the as-synthesized hierarchically structured self-cleaning surfaces, we employed the XPS technique to evaluate the effect of APP-treatment. As shown in Fig. S3, the full XPS spectra indicate that only tungsten, oxygen, and a small amount of carbon existed on the surface after treatment with oxygenand argon plasma. After surface modification with FAS, the treated sample exhibited obvious signals from fluorine, carbon, tungsten, and oxygen. Compared with the spectrum of a cleaned silicon wafer, the hierarchically structured textures were mainly composed of tungsten and oxygen. Moreover, FAS molecules were successfully deposited on the textured surfaces through the facile route at room temperature. Fig. 3a shows the in situ XPS for the as-synthesized porous structures with a two-tier topography after APP treatment. According to the fitting results, four W 4f characteristic peaks contributed from the surface of as-synthesized coating were detected. Two peaks were observed at 36.1 and 38.2 eV, corresponding to the valence of W^{6+}, and the other two peaks appeared at 37.1 and 34.7 eV, corresponding to that of W^{5+}.[36] After sputtering with an Ar^+ ion beam (3 kV, 2×2 raster) for 2 min, the intensity of the W^{6+} and W^{5+} peaks decreased substantially. The two peaks at 33.3 and 31.2 eV corresponded to metal tungsten[36] and remained high even after sputtering for 4 min. The corresponding sputtering depth of the porous tungsten oxide (WO_{3-x}) coating can be determined by the Si 2p core-level spectra (Fig. 3b). Due to the absence of the peak of Si 2p from SiO_2 at 103.6 eV and the increase of that from Si at 99.4 eV, the porous WO_{3-x} coatings were removed from the substrate after beam sputtering for 4 min. We discovered that the working gas with 0.2% of O_2/Ar during the plasma treatment enabled the deposition of both the fully oxidized tungsten (WO_3) and low oxidation state of WO_{3-x}, which is similar to the results of Yoshiki et al.[40] Furthermore, the in-situ XPS results clearly indicated the composition transition from WO_{3-x} to tungsten, revealing that the oxygen content decreased from the top to the bottom of the coatings. Based on optical emission spectroscopy analysis, the characteristic peaks detected from the APP jet within the wavelength of 400-500 nm were indexed as the atomic lines of tungsten[36] (Fig. S4). The intensities of selected characteristic peaks were all proportional to that of oxygen radicals. We concluded that the frequent collision between the tungsten electrode and oxygen radicals facilitated the growth of the porous WO_{3-x} layer. Without the injection of oxygen gas, no atomic lines of tungsten could be detected. The excited tungsten ions apparently transferred to tungsten through spontaneous redox reaction and self-assembled into a rough tungsten layer. Due to the subsequent supplement of oxygen flow and the elevated temperature caused by the APP jet, the as-synthesized porous tungsten layer was oxidized from the outer to the inner layers.

Multilayer Growth of FAS

To fabricate the self-cleaning WO_{3-x} (SCWO) coatings, a simple method was designed to effectively grow the multilayer of FAS at room temperature, which induced the Wenzel-Cassie transition toward water. A small amount of FAS liquid (4 μL) was added around the edge of the samples whose surfaces were all terminated with high density hydroxyl (OH) groups by the APP treatment. The vaporized FAS molecules (0.00187 mmHg, 25 ℃) reacted with water molecules in an ambient environment, thus triggered the hydrolysis reaction spontaneously. The three ethoxy groups of the FAS molecules formed hydroxylsilane groups , which possessed a higher affinity toward OH-bearing substrates than the precursors. Due to the formation of hydrogen bonding, the hydroxylsilane groups coupled to each other and with the OH-bearing porous WO_{3-x} coating.

R-Si-O-H + H-O-Me=RSi-O-Me+H_2O

As shown in the aforementioned reaction, the metallo-siloxane bonds (Me-O-Si) were created during the condensation reaction.[41] To investigate the effect of coating time regarding surface wettability, we characterized R_q and sectional profile by AFM, as shown in Fig. 4a. The average R_q of the OH-

bearing porous WO_{3-x} coating was measured to be 78 nm $\pm$ 6 nm. After coating for 1 h, the sample exhibited 46 % lower roughness than the initial value. The difference in the average R_q between the two conditions was much higher than the thickness of a self-assembled monolayer of FAS (approximately 1.1 nm).[42] This result clearly indicated that the network of cross-linked siloxane with Si-O-Si linkages self-assembled and formed a multi-layer coating along the topography of the deposited WO_{3-x} film. Furthermore, the roughness spacing (λ) progressively increased from 43.1 nm $\pm$ 11 nm to 334 nm $\pm$ 56.6 nm as the coating time increased. However, since the hierarchically rough surface feature was adequately preserved, the substrate modified with FAS for 1 h obtained superior superhydrophobicity and oleophobicity under the Cassie state (Fig. 4b). We demonstrated that the hydroxylsilane groups derived from FAS molecules underwent the horizontal polymerization as well as vertical condensation, which caused the formation of thick polysiloxane during the condensation process due to the high density of OH groups and hierarchicallyl structured topography.[41] When the coating time was further extended to 32 h, the surface was obviously flattened, thus losing non-wetting properties, and was accompanied by a decreased in SCA by 30° toward water as well as an increased sliding angle of up to 60°.

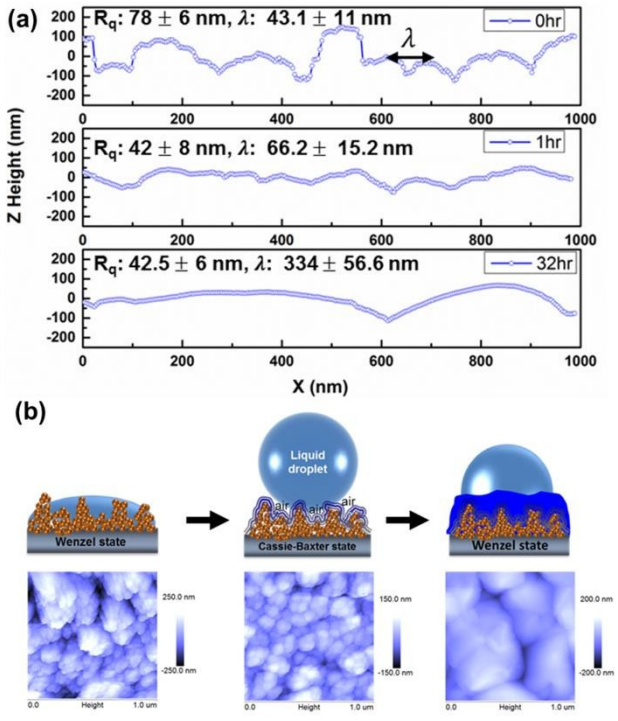

Fig. 4 (a) Roughness height, R_q, and rough spacing for porous WO_{3-x} coatings after varying coating durations measured by AFM. (b) AFM topography images (scanning size: 1×1 μm^2) and schematics of the Wenzel-Cassie-Wenzel transition caused by multilayer chemisorption of FAS as the coating time increased. In the schematics, the brown particles are the WO_{3-x} nanoparticles which aggregated together and formed stalagmite-like protrusions. The blue triple line is the multi-layer FAS after 1 h of FAS vapor deposition. The royal blue bulk right beneath the liquid droplet are the thick FAS multi-layer film after depositing for 32 h.

Dynamic Behaviour of Water Droplets on SCWO Surfaces

To evaluate the anti-adhesive property of the SCWO-coated sueface toward water, we used a high speed camera to record the dynamic behavior of a bouncing drop striking the SCWO-coated surface. Side view and top view images (Fig. S5a and Fig. S5b) showed that the bouncing drop (initial radius R = 1.23 mm, impact velocity v_0 = 1.72 ms^{-1}, corresponding to Weber number $We = 50.2$, where $We \equiv \rho v_0^2 R/\gamma$, with ρ being the liquid density and γ being the liquid-air surface tension) completely detached from the surface at the first bounce after 10.2 ms, which was defined as the contact time (t_c). We converted t_c on the basis of other experiments into the dimensionless time t_c/τ because t_c is affected by the inertia-capillary timescale ($\tau \equiv \sqrt{\rho R^3/\gamma}$).[43-45] In our experiment, t_c of SCWO-coating was approximately 2, which is 10 % less than that for typical superhydrophobic surfaces (Table S2). Thus, the SCWO-coating may act as an efficient material for self-cleaning applications. Moreover, to explore and quantify the ability to reduce the frictional force, we fabricated SCWO coatings on curved polyethylene terephalate (PET) substrates (Fig. S5c). A thin layer of SCWO coating performed with remarkable flexibility and transparency. Fig. S5d further shows the calculated trajectory of the water droplet rolling on curved SCWO-coated PET film. The water droplet (7.7 μL) completed at least five cycles before it completely stopped. The calculated energy dissipation for each half cycle of a water droplet, on average, was only 15.3% as mentioned in Table S3, whereas the water droplet tightly adhered to the surface of a normal PET film.

To further explore potential applications, the long-term stability and thermal resistance of the coatings in open air were investigated. To evaluate the long-term stability, the SCWO-coated glass substrates were stored in a Petri dish at room temperature for up to 16 days. The corresponding SCA toward water with regard to the aging time were recoded (Fig. 5a). The results indicated that the substrate without FAS modification exhibited stable superhydrophilicity because of asperities on the rough surface and coordination unsaturation on the surface of WO_{3-x} as common metal oxide.[9] Consequently, the coating showed long-term superhydrophilicity, although the OH groups deposited by the APP technique degraded with time. By contrast, the FAS-modified SCWO coatings showed high SCA (161.3° $\pm$ 2.4°) and satisfactory aging stability. The thermal resistance was determined by annealing the coated glass at elevated temperatures from 120℃ to 360 ℃ for 1 h as shown in Fig. 5b. The SCA toward water remained constant for temperatures up to 325℃, and the water droplet readily rolled off the surface with < 1° sliding angle. Fig. S6 and S7 show the TGA curves of the modified glass and the precursor of the FAS, respectively. The results displayed that, without polymerization, the weight loss percentage of the FAS precursors was approximately 80% when heated to 300℃. However, the modified glass exhibited 0.2 % $\pm$ 0.1 % weight loss, which was mainly contributed by the cross-linked siloxane, only when the temperature achieved within 330 to 380 ℃. We attributed the enhanced reliability to the strong carbon-fluorine bonding and covalent bonding between hydroxylsilane groups and the surface of substrates, which effectively prevented from the oxidation in the ambient atmosphere.[24] After heating up to 360 ℃, the SCA toward water significantly decreased to < 10° due to the detachment of the FAS multilayeron the textured surface. Therefore, the substrate coated with hierarchically structured tungsten oxide became superhydrophilic again.

Some studies have proposed that FAS may not be the optimal choice for providing a long-term stability of hydrophobicity in contact with water.[46, 47] The metallo-siloxane bonds were gradually hydrolyzed back to the silano groups when in contact with water molecules for a sufficient duration. Although the surface density of the alkyl chains was increased by the buffer layers that provided more OH groups, the capability of the two-layer samples for resisting the penetration of water molecules were extremely limited.[46] To investigate the long-term durability for prolonged continuous exposure of SCWO coatings to water, two kinds of samples, SCWO-coated glasses and FAS-multilayer-coated glasses with a flat surface (i.e. the deposition time of FAS was long enough to flatten the surface textures), were placed inside the chamber under 97 % humidity atmosphere. The evolution of SCA toward water on the tested samples were evaluated through in-situ SCA measurement (Fig. 5c). The SCWO-coated glasses (black sqaures) demonstrated higher SCA than that on flat FAS-multilayer-coated glasses (red circles) because of the rough surface textures. The SCA of flat FAS-multilayer-coated glasses did not appear to change after 192 h, whereas that of SCWO-coated glasses slightly decreased from 161.2° ± 1.8° to 151.4° ± 2.6° after 168 h. Based on these results, the FAS deposited on SCWO-coated glasses were believed to gradually hydrolyze under a high humidity environment, thus the asperities of the samples exhibited higher affinity toward water (Fig. 5d). Accordingly, SCWO-coatings were not infinetly stable for prolonged continuous exposure to water. Systematic designs to improve the physical and chemical properties of the SCWO coating against high humidity environment are in progress.

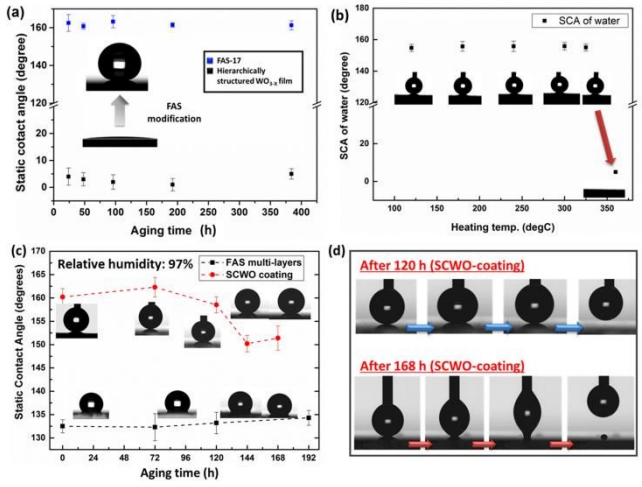

Fig. 5 (a) The aging stability of SCWO coatings before and after FAS vapor modification in an ambient environment. (b) Thermal resistance of SCWO coatings evaluated through the measurement of SCA toward water under various temperatures. Long-term durability test under high humidity environment for two types of FAS-coated glass evaluated through (c) the evolution of SCA as the aging time increased, and (d) the adhesion between pendant water drop and SCWO-coating after different durations.

Nevertheless, the degradation rate of anti-wettability under a high humidity environment may be effectively reduced through increasing the thickness of multi-layer FAS. The topmost of FAS acted as a sacrificing layer to protect the surface beneath. When contacting with water or humidity, the topmost layer partially hydrolyzed and uncovered a fresh surface beneath to repel water or low-surface tension liquids. In addition, some previous studies[48-51] indicated that rough superhydrophobic surfaces that sustained the mechanical stress during ice detachment or long-term icing/deicing cycles are rare. The ice adhesion increased obviously when asperities of surface were destroyed. Accordingly, FAS-multilayer-coated substrates with a relatively flat surface should exhibit better long-term durability against water and ice than SCWO coatings when applied for anti-icing applications.

Transparent and self-cleaning properties are tempting for many applications, such as electronic devices, windows, and solar panels. The SCWO-coated glass was demonstrated to have satisfactory self-cleaning ability, as shown in the supplementary video S2. The sands sprayed on the surface of the coated glass could be readily removed by rolling water droplets. In addition, the self-cleaning properties were well-preserved (within < 5° of sliding angle) even after performing the sand abrasion tests designed by Xu et al.,[4] as shown in supplementary videos S3 and S4 demonstrating the excellent mechanical properties against dynamic wear on the SCWO coatings.

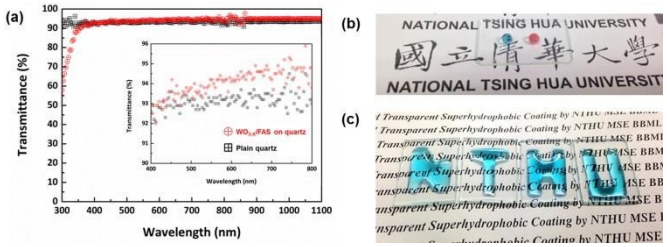

Fig. 6 (a) UV-Vis-NIR spectra of SCWO-coated quartz substrate compare with that of plain quartz. (b) Photograph of high contact angles of blue-dyed water and red-dyed n-Hexadecane deposited on SCWO-coated glass. (c) Photograph of a glass with untreated hydrophilic characters "NTHU" and coated superhydrophobic surrounding.

UV-Vis-NIR spectra of plain quartz and SCWO-coated quartz are shown in Fig. 6a. The coated quartz possessed higher transmittance than the plain quartz did. The transmittance of the coated quartz ranged from 93% to 96% in the range of 600 to 1000 nm (red circle) and exhibited a maximum transmittance at 786 nm, whereas the transmittance of the plain quartz was approximately 93 % (black square). The transmittance of the coated quartz was lower than that of the plain quartz below 350 nm because of light scattering. By neglecting the reflection from the interfaces and the thin-film interference effect, the effective refractive index of the porous SCWO can be determined by eq (1) as follows:

$$T = 1 - \left(\frac{1-n_f}{1+n_f}\right)^2 - \left(\frac{n_f - n_q}{n_f + n_q}\right)^2 + \left[\frac{n_q - 1}{n_q + 1}\right]^2 \quad (1)$$

where T is the transmittance. n_f represents the effective refractive index of the SCWO coating, and n_q (= 1.446) depicts the refractive index of plain quartz. For instance, when T equals 95% at λ = 1000 nm, the effective refractive index of the SCWO coating can be calculated to be 1.2, which was 43% lower than that of a dense WO_{3-x} film (n ≅ 2.1).[52] The reduced index of the porous WO_{3-x} and air interface compared with that of the original quartz/air interface contributed to the enhanced transmittance of the SCWO coating. The highly transparent SCWO-coated glass (Fig. 6b) provided satisfactory readability of the underneath letters.

To demonstrate the capability of fabricating hydrophilic/superhydrophobic patterns, a polyimide film silicone tape (3M™ Polyimide Film Tape 5413) was used to shield the regions on the well-cleaned glass. After the APP process and selective FAS deposition, the shielded region remained hydrophilic due

to the intrinsic property of the glass (SiO_2), whereas the remaining substrate exhibited superhydrophobicity, which was capable of pinning the blue-dyed water on the surface to reveal the characters "NTHU"(Fig. 6c).

In addition, the versatility of the SCWO coating was demonstrated by modifying paper with a thin layer of SCWO coating. The treated paper effectively resisted the blue-dyed water droplet from penetrating through the substrate (Fig. 7a and top of 7b) and no impalement was observed (*We*= 11.7). However, the normal paper was soaked by water within a few milliseconds (bottom of Fig. 7b). The corresponding SEM images of treated and un-treated papers are shown in Fig. 7c and 7d. Clearly, the cellulose fibers of the treated paper were uniformly covered with WO_{3-x} protrusions terminated with multi-layer FAS, which entrapped air cushions that prevented moistening by the water droplets. Based on these results, we demonstrated the synergistic effect of the two-tier topography of the WO_{3-x} and multi-layer FAS molecules contributing to stable superhydrophobicity and oleophobicity on various substrates.

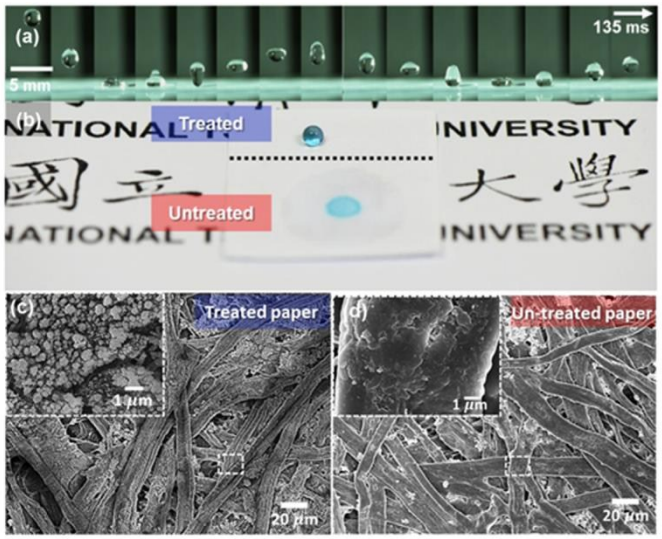

Fig. 7 (a) Time-resolved images taken by high speed camera reveal a water bouncing drop on the SCWO-coated paper. (b) Photograph of the anti-wettability comparison for the SCWO-coated and uncoated papers. The coated-paper cannot moisten with the blue-dyed water. SEM images of (c) SCWO-coated paper and (d) normal paper.

Conclusions

In conclusion, we demonstrated a simple and versatile strategy for fabricating an effective and transparent self-cleaning coating. Because the process is rapid under ambient gas pressure and at room temperature, the two-tier porous WO_{3-x} nanoparticles and micro-agglomeration as well as the multilayer chemisorption of FAS were developed on various substrates. This combination performs robust Cassie state wetting toward water and glycerol and allows the contact time at first bouncing of water to decrease 10%. The SCWO coating is a potential candidate for an effective self-cleaning coating in both indoor and outdoor environment. In addition, our coating exhibited substantial thermal-stability up to 325 ℃ and showed no performance deterioration under open-air conditions for at least one month. Moreover, the excellent transmittance of the SCWO coating was verified within visible light and near-infrared regions. The self-cleaning ability was maintained and reproducible even after sand abrasion. Furthermore, the robust SCWO coating effectively reduced the adhesion force between a water droplet and the PET film. The hierarchically-structured, transparent, SCWO coatings, which were synthesized through this facile route, revealed outstanding liquid repellence and cost-effectively multifunctional surfaces as well.

Acknowledgements

Authors sincerely thank the financial support from the Ministry of Science and Technology, Taiwan (MOST101-2628-E-007-017-MY3, MOST102-2221-E-007-045-MY3 and MOST103-2221-E-007 -034-MY3), Precious Instrument Utilization Center sponsored by the MOST, and the Industrial Technology Research Institute (ITRI-MCL-D254W0B100).

Notes and references

1. Y. Tian, B. Su and L. Jiang, *Adv. Mater.*, 2014, **26**, 6872-6897.
2. L. Yao and J. He, *Prog. Mater Sci.*, 2014, **61**, 94-143.
3. K.-C. Park, H. J. Choi, C.-H. Chang, R. E. Cohen, G. H. McKinley and G. Barbastathis, *ACS Nano*, 2012, **6**, 3789-3799.
4. X. Deng, L. Mammen, Y. Zhao, P. Lellig, K. Müllen, C. Li, H.-J. Butt and D. Vollmer, *Adv. Mater.*, 2011, **23**, 2962-2965.
5. S. Pan, A. K. Kota, J. M. Mabry and A. Tuteja, *J. Am. Chem. Soc.*, 2012, **135**, 578-581.
6. L. Wen, Y. Tian and L. Jiang, *Angew. Chem. Int. Ed.*, 2015, **54**, 3387-3399.
7. W. Barthlott and C. Neinhuis, *Planta*, 1997, **202**, 1-8.
8. Y. Tian and L. Jiang, *Nat. Mater*, 2013, **12**, 291-292.
9. G. Azimi, R. Dhiman, H.-M. Kwon, A. T. Paxson and K. K. Varanasi, *Nat. Mater*, 2013, **12**, 315-320.
10. D. Bonn, J. Eggers, J. Indekeu, J. Meunier and E. Rolley, *Rev. Mod. Phys.*, 2009, **81**, 739-805.
11. J. Adams and D. Pendlebury, *Global Research Report: Materials Science and Technology*, Global Research Report: Materials Science and Technology, Thomson Reuters ScienceWatch, 2011.
12. J. Ju, H. Bai, Y. Zheng, T. Zhao, R. Fang and L. Jiang, *Nat. Commun*, 2012, **3**, 1247.
13. K. Li, J. Ju, Z. Xue, J. Ma, L. Feng, S. Gao and L. Jiang, *Nat. Commun*, 2013, **4**, 2276.
14. D. Quéré, *Annu. Rev. Mater. Res.*, 2008, **38**, 71-99.
15. A. Tuteja, W. Choi, M. Ma, J. M. Mabry, S. A. Mazzella, G. C. Rutledge, G. H. McKinley and R. E. Cohen, *Science*, 2007, **318**, 1618-1622.
16. H. Bellanger, T. Darmanin, E. Taffin de Givenchy and F. Guittard, *Chem. Rev.*, 2014, **114**, 2694-2716.
17. T.-S. Wong, S. H. Kang, S. K. Y. Tang, E. J. Smythe, B. D. Hatton, A. Grinthal and J. Aizenberg, *Nature*, 2011, **477**, 443-447.
18. K. Golovin, D. H. Lee, J. M. Mabry and A. Tuteja, *Angew. Chem. Int. Ed.*, 2013, **52**, 13007-13011.
19. A. K. Kota, G. Kwon and A. Tuteja, *NPG Asia Mater*, 2014, **6**, e109.
20. N. Vogel, R. A. Belisle, B. Hatton, T.-S. Wong and J. Aizenberg, *Nat. Commun*, 2013, **4**, 2176.

21. L. Xu, R. G. Karunakaran, J. Guo and S. Yang, *ACS Appl. Mater. Interfaces*, 2012, **4**, 1118-1125.
22. X. Deng, L. Mammen, H.-J. Butt and D. Vollmer, *Science*, 2012, **335**, 67-70.
23. J.-H. Kong, T.-H. Kim, J. H. Kim, J.-K. Park, D.-W. Lee, S.-H. Kim and J.-M. Kim, *Nanoscale*, 2014, **6**, 1453-1461.
24. A. Irzh, L. Ghindes and A. Gedanken, *ACS Appl. Mater. Interfaces*, 2011, **3**, 4566-4572.
25. C.-H. Xue and J.-Z. Ma, *J. Mater. Chem. A*, 2013, **1**, 4146-4161.
26. L. Cao, A. K. Jones, V. K. Sikka, J. Wu and D. Gao, *Langmuir*, 2009, **25**, 12444-12448.
27. V. A. Ganesh, H. K. Raut, A. S. Nair and S. Ramakrishna, *J. Mater. Chem.*, 2011, **21**, 16304-16322.
28. L. Mishchenko, B. Hatton, V. Bahadur, J. A. Taylor, T. Krupenkin and J. Aizenberg, *ACS Nano*, 2010, **4**, 7699-7707.
29. Y.-Y. Ji, S.-S. Kim, O. P. Kwon and S.-H. Lee, *Appl. Surf. Sci.*, 2009, **255**, 4575-4578.
30. R. Hensel, R. Helbig, S. Aland, A. Voigt, C. Neinhuis and C. Werner, *NPG Asia Mater*, 2013, **5**, e37.
31. A. Hirao, K. Sugiyama and H. Yokoyama, *Prog. Polym. Sci*, 2007, **32**, 1393-1438.
32. T. Darmanin, E. T. de Givenchy, S. Amigoni and F. Guittard, *Adv. Mater.*, 2013, **25**, 1378-1394.
33. H.-J. Choi, S. Choo, J.-H. Shin, K.-I. Kim and H. Lee, *J. Phys. Chem. C*, 2013, **117**, 24354-24359.
34. T. Young, *Phil. Trans. R. Soc. Lond.*, 1805, **95**, 65-87.
35. E. F. Hare, E. G. Shafrin and W. A. Zisman, *J. Phys. Chem.*, 1954, **58**, 236-239.
36. J. Wang and C. K. Ober, *Macromolecules*, 1997, **30**, 7560-7567.
37. T. Verho, J. T. Korhonen, L. Sainiemi, V. Jokinen, C. Bower, K. Franze, S. Franssila, P. Andrew, O. Ikkala and R. H. A. Ras, *Proc. Natl. Acad. Sci. U.S.A.*, 2012, **109**, 10210-10213.
38. M. Davide and R. M. Sankaran, *J. Phys. D: Appl. Phys.*, 2010, **43**, 323001.
39. Y. Shimizu, T. Sasaki, A. Chandra Bose, K. Terashima and N. Koshizaki, *Surf. Coat. Technol.*, 2006, **200**, 4251-4256.
40. S. Yoshiki, B. Arumugam Chandra, M. Davide, S. Takeshi, K. Kazuhiro, S. Tsunehisa, T. Kazuo and K. Naoto, *Jpn. J. Appl. Phys.*, 2006, **45**, 8228.
41. M. Akram Raza, E. S. Kooij, A. van Silfhout and B. Poelsema, *Langmuir*, 2010, **26**, 12962-12972.
42. B. C. Bunker, R. W. Carpick, R. A. Assink, M. L. Thomas, M. G. Hankins, J. A. Voigt, D. Sipola, M. P. de Boer and G. L. Gulley, *Langmuir*, 2000, **16**, 7742-7751.
43. D. Richard, C. Clanet and D. Quere, *Nature*, 2002, **417**, 811-811.
44. J. C. Bird, R. Dhiman, H.-M. Kwon and K. K. Varanasi, *Nature*, 2013, **503**, 385-388.
45. Y. Liu, L. Moevius, X. Xu, T. Qian, J. M. Yeomans and Z. Wang, *Nat Phys*, 2014, **10**, 515-519.
46. S. A. Kulinich, M. Honda, A. L. Zhu, A. G. Rozhin and X. W. Du, *Soft Matter*, 2015, **11**, 856-861.
47. W. J. van Ooij, D. Zhu, M. Stacy, A. Seth, T. Mugada, J. Gandhi and P. Puomi, *Tsinghua Sci. Technol.*, 2005, **10**, 639-664.
48. L. B. Boinovich, A. M. Emelyanenko, V. K. Ivanov and A. S. Pashinin, *ACS Appl. Mater. Interfaces*, 2013, **5**, 2549-2554.
49. S. A. Kulinich and M. Farzaneh, *Cold Reg. Sci. Technol.*, 2011, **65**, 60-64.
50. S. A. Kulinich, S. Farhadi, K. Nose and X. W. Du, *Langmuir*, 2011, **27**, 25-29.
51. A. Lazauskas, A. Guobienė, I. Prosyčevas, V. Baltrušaitis, V. Grigaliūnas, P. Narmontas and J. Baltrusaitis, *Mater. Charact.*, 2013, **82**, 9-16.
52. C. Charles, N. Martin, M. Devel, J. Ollitrault and A. Billard, *Thin Solid Films*, 2013, **534**, 275-281.

Robust stalagmite-like self-cleaning surfaces with good transparency and flexibility are developed by plasma-assisted nanofabrication and silanization at ambient condition.